mental data, the frequencies of transverse phonons (700 cm^{-1}) and longitudinal oscillations (890 cm^{-1}), as well as their oscillator strengths, were obtained for 1- and 2-nm-thick AlN films [8] and for 25- and 400-nm-thick AlN films on sapphire [9].

It would seem that follow-up studies of the optical characteristics of AlN during monolayer-by-monolayer growth would provide answers to very important questions, namely, how the AlN layers are formed, how their characteristics change due to great stresses in them caused by a large mismatch between lattice constants, and how the surface layers of sapphire are transformed.

Unfortunately, direct surface-nonperturbing methods for measuring the fluctuating fields of surface electromagnetic excitations are absent at present, and the near-field spectroscopy (in the ATR regime) appears to be the most 'delicate' technique for studying the surface of crystals and thin films deposited on them.

4. Conclusion

Correct measurements of ATR spectra for many angles of incidence of light inside a prism make ATR spectroscopy, in fact, a quantitative technique for measuring the permittivity of ultrathin films, including monolayer films, in which the concept of the macroscopic permittivity appears inapplicable. Nevertheless, as is seen from the results presented above, 10-nm-thick MgO film and 1- and 2-nm-thick AlN films are well described by the standard model of the permittivity of bulk MgO and AlN, respectively.

In this paper, we have studied the resonance interaction of the substrate SPs with optical phonons in films and measured the splitting of SP dispersion curves. This splitting was proved to be proportional to the square root of the film thickness. It is shown that the ATR spectroscopy can be utilized for determining the permittivity of thin and ultrathin films.

Acknowledgments

The authors thank G Rossetto, A Sartori, and M Bolzan (Instituto di Chimica Inorganica e delle Superfici, Padova, Italy) for preparing samples with MgO films on sapphire, and K S Zhuravlev, V G Mansurov, and T V Malin (Rzhanov Institute of Semiconductor Physics, Siberian Branch of the Russian Academy of Sciences), and S S Ng, Z Hassan, and H Abu Hassan (School of Physics, University Sains Malaysia) for preparing samples with AlN films on sapphire. The work was supported by a grant from the Program of Fundamental Research of the Physical Sciences Division, RAS entitled 'Physics of New Materials and Structures', and by a grant No. 11-02-00325a from the Russian Foundation for Basic Research.

References

1. Vinogradov E A, Dorofeyev I A *Phys. Usp.* **52** 425 (2009); *Usp. Fiz. Nauk* **179** 449 (2009)
2. Dorofeyev I A, Vinogradov E A *Phys. Rep.* **504** 75 (2011)
3. Dorofeyev I A, Vinogradov E A *Laser Phys.* **23** 065903 (2013)
4. Zhizhin G N et al. *Appl. Spectrosc. Rev.* **18** (2) 171 (1982)
5. Oura K et al. *Surface Science: An Introduction* (Berlin: Springer-Verlag, 2003)
6. Agranovich V M, Malshukov A G *Opt. Commun.* **11** 169 (1974)
7. Yakovlev V A et al. *J. Nanopart. Res.* **13** 5841 (2011)
8. Novikova N N et al. *Surf. Coat. Technol.* **227** 58 (2013)
9. Yakovlev V A et al. *Phys. Lett. A* **373** 2382 (2009)
10. Vinogradov E A *Phys. Usp.* **45** 1213 (2002); *Usp. Fiz. Nauk* **172** 1371 (2002)
11. Vinogradov E A, Dorofeyev I A *Termostimulirovannye Elektromagnitnye Polya Tverdykh Tel* (Thermally Stimulated Electromagnetic Fields of Solids) (Moscow: Fizmatlit, 2010)
12. Barker A S (Jr.) *Phys. Rev.* **132** 1474 (1963)

PACS numbers: 42.50.Ex, **42.81.–i**, **78.67.–n**
DOI: 10.3367/UFNe.0184.201406h.0656

Quantum control of atoms and photons by optical nanofibers

V I Balykin

1. Introduction

Studies of the interaction of light with matter at the level of single atoms and photons not only provide a deeper understanding of the quantum-mechanical nature of the light–matter interaction but also open up prospects for new quantum technologies. During the last two decades, quite a few approaches have been adopted for realizing interaction at the level of single atoms and photons. The possibility of achieving single-particle interaction is basic to the concept of quantum information processing and communication [1, 2]: atoms are treated as physical objects that can store and process information, and photons as objects for long-range data transmission through a quantum information network. The quantum information network can comprise, for instance, single atoms (ions, molecules, or quantum dots) representing addressable points of the quantum information network and optical (or other) waveguides providing photon-assisted effective connections among nodes of the quantum information network.

At present, the efficient coupling of single photons with an atomic medium is achieved on a basis of the following physical mechanisms: (1) the microscopic localization of single atoms and the attainment of the 'strong interaction' regime [3, 4]; (2) the use of laser fields focused to light spots comparable in size to the absorption cross section of a single atom [5–8], and (3) the employment of coherent coupling with optically thick atomic ensembles [2]. Despite the outstanding achievements obtained by these methods, a simple, reliable, and scalable technique for the integration of simple quantum systems with photon systems has been lacking.

In this paper, we will briefly review the work on the deterministic control of single atoms and single photons, and on establishing conditions for their efficient interaction. Such a control based on the use of *ultracold atomic ensembles near an optical nanowaveguide* was first proposed a decade ago by Balykin et al. [9]. The subsequent experimental realizations of a hybrid (atom + nanowaveguide) system [10–12] have demonstrated the outlook for its use in a variety of applica-

V I Balykin Institute of Spectroscopy, RAS, Troitsk, Moscow, Russian Federation
E-mail: balykin@isan.troitsk.ru

Uspekhi Fizicheskikh Nauk **184** (6) 656 – 665 (2014)
DOI: 10.3367/UFNr.0184.201406h.0656
Translated by M Sapozhnikov; edited by A Radzig

tions. A hybrid (atom + nanowaveguide) system offers three main advantages over other systems:

(i) a great fraction of photons emitted by atoms is captured by a mode of the nanowaveguide and is then channeled along the waveguide [13]. This, in turn, opens up the possibility of efficient detection (free from parasitic noise, which is important from the experimental point of view) of radiation from a single atom;

(ii) an atom and a photon in the hybrid system are located in a region with the transverse size smaller than the diameter of the absorption cross section of the atom, i.e., an optically dense medium with one or a few atoms is realized [14]. This, in turn, offers ample scope for realizing parametric processes with matter at the level of *several atoms* and light at the level of *several photons* [15];

(iii) the hybrid (atom + nanowaveguide) system allows one to realize the efficient radiative exchange between single atoms separated by *large distances* via the nanowaveguide mode [13, 16, 17]. Such a system is considered to be an elementary building block in a quantum information network.

2. Localization of light in a dielectric nanowaveguide

Optical nanowaveguides (up to 50 nm in diameter) were first fabricated and studied by Mazur's group [18]. They demonstrated the unique physical and optical properties of these nanowaveguides and pointed out an ample scope of their possible application. Figure 1 shows schematically a nanowaveguide — a dielectric cylinder of a nanometer radius.

The optical characteristics of a nanowaveguide depend on its radius a and the wavelength of light. If the condition $V = ka(n_1^2 - n_2^2)^{1/2} < V_c = 2.405$ is fulfilled, where n_1 is the refractive index of the waveguide material, and n_2 is the refractive index of the environment material, the nanowaveguide contains only one fundamental HE_{11} mode [19] ($k = 2\pi/\lambda$, λ is the radiation wavelength). The electromagnetic field of the fundamental mode is strongly bounded in space, with a part of the light field outside the nanowaveguide rapidly decaying with distance from the waveguide surface. The spatial dependence of the field amplitude outside the nanowaveguide is described by the modified Bessel function $K_0(qr)$. The field outside the nanowaveguide decays on the characteristic length $l = 1/q$, the parameter q being determined from the solution of the equation for the eigenvalues of the waveguide.

Figure 2a depicts the field intensity distribution for the fundamental mode of the nanowaveguide as a function of the distance from the waveguide center for quasilinearly polarized light (the waveguide radius is $a = 0.2$ μm, the wavelength is $\lambda = 1.3$ μm, $n_1 = 1.4469$, and $n_2 = 1$). For these typical parameters of the nanowaveguide, the characteristic spatial size of the light field outside the waveguide is considerably smaller than the wavelength of light.

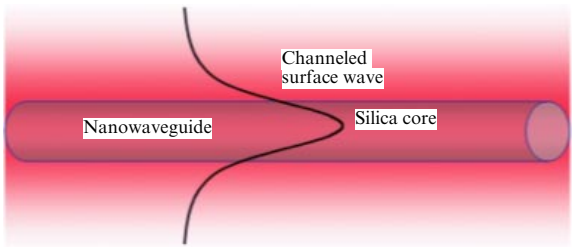

Figure 1. Dielectric nanowaveguide and the light field of the fundamental waveguide mode.

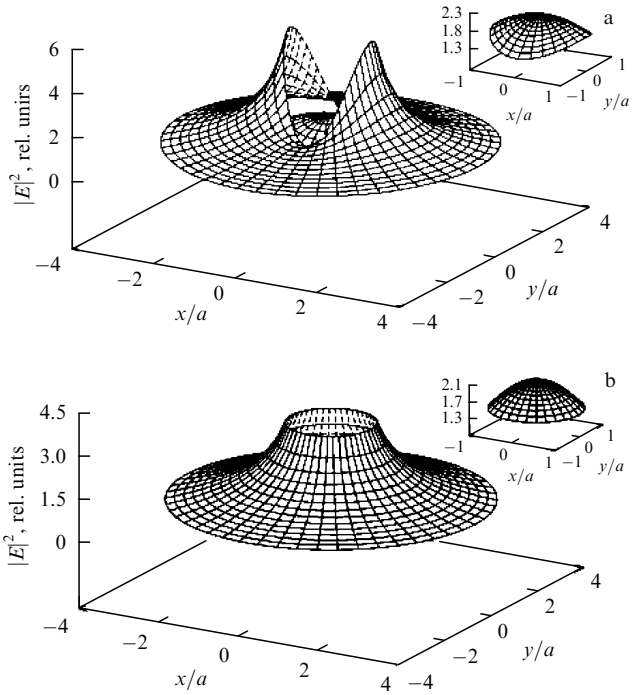

Figure 2. (a) Field intensity distribution profile for the fundamental HE_{11} mode of a nanowaveguide for the case of linear polarization [19]. The inset shows the field distribution inside the nanowaveguide. The nanowaveguide parameters are as follows: radius $a = 0.2$ μm, wavelength $\lambda = 1.3$ μm, $n_1 = 1{,}4469$, and $n_2 = 1$. (b) Field intensity distribution profile for the fundamental mode of the nanowaveguide for the case of circular polarization [20]. The inset shows the field distribution inside the nanowaveguide.

One can see from Fig. 2 that the light field distributions inside and outside the nanowaveguide are different. First, the field strength experiences discontinuity on the waveguide surface. Second, the spatial field distribution does not possess cylindrical symmetry in the case of linear polarization. For circular polarization, the field distribution of the fundamental mode already has cylindrical symmetry, but the field discontinuity on the waveguide surface is preserved (Fig. 2b).

The light field of the nanowaveguide is concentrated near its surface at distances smaller that the wavelength of light. The transverse compression of the field achieves the maximum for the radius–wavelength ratio $a/\lambda = 0.23$. The effective area of the field mode is comparable to the absorption cross section of an atom $\sigma \approx 3\lambda^2/(2\pi)$, which means that the atom can be efficiently coupled with the light field of the waveguide. Such a strong transverse compression of the field near the waveguide provides a high field strength, even for the low power of radiation coupled to the waveguide.

In the case of circular polarization [20], the electric field vector outside the waveguide has three components: the radial (E_r), azimuthal (E_ϕ), and longitudinal (E_z). The Poynting vector component corresponds to each of the components of the electric field vector: the radial (S_r), azimuthal (S_ϕ), and longitudinal (S_z), which are responsible for the transfer of energy, linear and angular momenta of the electromagnetic field.

As shown in Ref. [20], the electromagnetic field of the nanowaveguide possesses, unlike light in free space, both the orbital and spin components of the angular momentum. The linear momentum density for the electromagnetic field in free space is determined by the expression $\mathbf{p}_{\text{local}} = \mathbf{S}/c^2$. For the field in a dielectric medium, several definitions of the linear momentum density exist. In the Abraham formulation, the linear momentum density is described by the expression $\mathbf{p}_{\text{local}} = \mathbf{E} \times \mathbf{H}/c^2$, while in the Minkowski formulation it is described by the expression $\mathbf{p}_{\text{local}} = \mathbf{D} \times \mathbf{B}$. Although this question is not finally solved, as a rule, the Abraham formulation is considered preferable [21, 22].

The light field propagates in the nanowaveguide in both dielectric and free spaces. This opens up the possibility of arranging experiments to determine which of the definitions of the linear momentum density is correct.

The authors of paper [20] calculated the angular momentum of a photon propagating in a nanowaveguide as a function of the waveguide radius. It was shown that, according to the Abraham formulation, the value of no single component of the angular momentum exceeds Planck's constant $\hbar$: j, j_{sp}, $j_{\text{orb}} \leqslant \hbar$. If the radius of the nanowaveguide is small, the two components j and j_{sp} tend to their maximum values equal to $\hbar$, while the component j_{orb} tends to zero.

According to the Minkowski concept, the angular momentum of a photon in a dielectric and vacuum is the same, being equal to $\hbar$. For a nanowaveguide, according to Minkowski, the total angular momentum is independent of the waveguide radius: $j = \hbar$, and the spin and orbital components, j_{sp} and j_{orb}, of the angular momentum of a photon depend on the waveguide radius. The maximum value of the orbital component of the angular momentum equals $0.18\hbar$. The orbital component is maximum for a nanowaveguide with a diameter on the order of half the wavelength. In the case of an arbitrary radius of the waveguide, the spin component of the angular momentum dominates for nanowaveguides with radii smaller and larger than the wavelength of light.

As is known [23, 24], the angular momentum of light can be imparted to an atom interacting with radiation. Such a transfer of the angular momentum not only changes the internal state of the atom (optical pumping, orientation), but can cause the rotational motion of the atom [25].

3. Localization of an atom in the light field of a nanowaveguide

To date, two schemes for the localization of an atom by the light field of a nanowaveguide have been proposed [9, 26, 27], called the single-frequency and two-frequency schemes.

3.1 Localization of an atom by a single-frequency light field

Figure 3 illustrates the geometry of atomic localization in a *single-frequency* light field of the fundamental mode HE_{11} of a nanowaveguide [9]. The light field outside the waveguide produces an optical potential for the atom near the waveguide surface. When the frequency detuning of the light field is negative with respect to the atomic transition frequency, the potential is negative and the atom is pulled into the strong field region, which is located on the waveguide surface in this case. To provide the stable localization of the atom outside the waveguide surface, it is necessary to hold the atom at some distance from the waveguide surface. This can be achieved using the centrifugal force of the rotational motion of the atom around the nanowaveguide. It is well known that the centrifugal potential can compensate for the attractive potential decreasing with distance faster than r^{-2}.

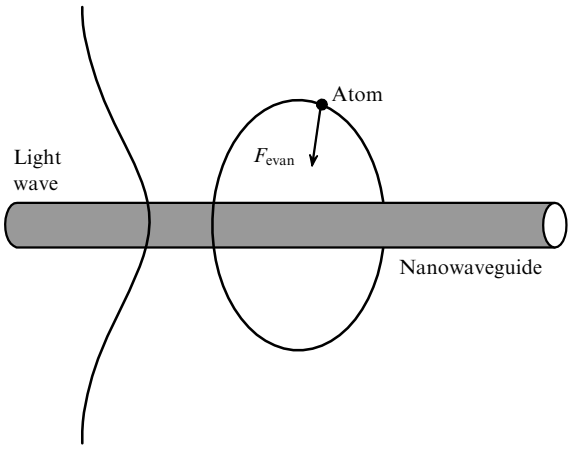

Figure 3. Schematic of atomic localization by a single-frequency light field of the fundamental waveguide mode. F_{evan} is the light pressure force acting on the atom in the surface wave field.

The light field outside the waveguide decays exponentially; therefore, the optical potential (for strong detuning of the field frequency from the atomic transition frequency) varies in the same fashion. This means that the centrifugal potential can be employed for the stable localization of the atom near the nanowaveguide.

If we assume that the optical potential U has cylindrical symmetry, U depends only on the distance r of the atom from the symmetry z-axis of the waveguide. Due to such a symmetry, the component L_z of the angular momentum of the atom is preserved and can be expressed as $L_z = -\hbar m$, where m is an integer called the rotational quantum number. The centrifugal potential is repulsive and can be written out in the form

$$U_{\text{cf}} = \frac{\hbar^2(m^2 - 1/4)}{2Mr^2}\,, \tag{1}$$

where M is the atomic mass. The radial motion of the atom can be considered as the one-dimensional motion of a particle in the effective potential $U_{\text{eff}} = U_{\text{cf}} + U$. The light field outside of a waveguide supporting only one fundamental HE_{11} mode is described by the modified Bessel function $K_0(qr)$, and the optical potential can be expressed in the form

$$U = -GK_0^2(qr)\,, \tag{2}$$

where $G = -\hbar\Omega_a^2/\Delta K_0^2(qa)$ is the coupling constant between the atom and light field, Ω_a is the Rabi frequency on the waveguide surface, and Δ is the frequency detuning of the light field.

The effective potential for the radial motion can be written in the form

$$U_{\text{eff}}(r) = R_{\text{rec}}\left(\frac{m^2 - 1/4}{k^2r^2} - gK_0^2(qr)\right), \tag{3}$$

where $R_{\text{rec}} = (\hbar k)^2/(2M)$ is the recoil energy, $g = G/R_{\text{rec}}$ is the normalized coupling constant, and m is an integer. The stable bound states of the atom near the waveguide are

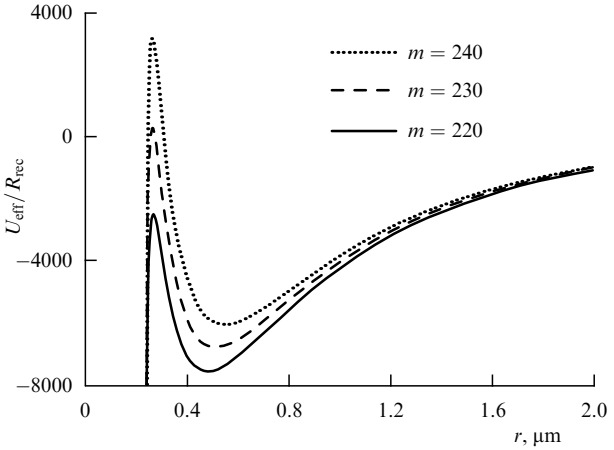

Figure 4. Effective potentials near the nanowaveguide, calculated taking into account the van der Waals force, for three quantum numbers m indicated in the figure [9]. The potential minimum is located at a distance equal to half the waveguide radius. The waveguide is made of silica, the wavelength is 1.3 μm, and the waveguide radius is 0.2 μm.

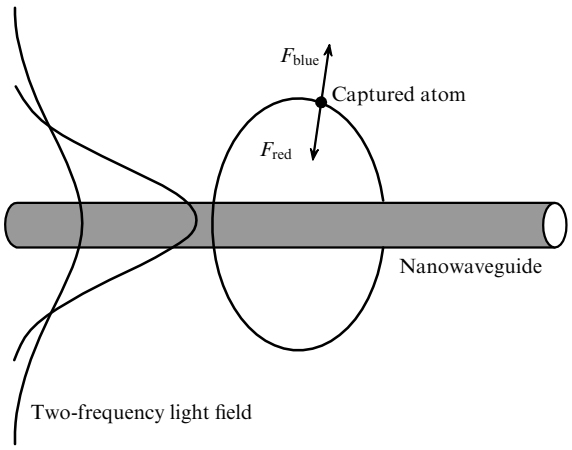

Figure 5. Schematic of atomic localization by a two-frequency light field: $F_{\rm blue}$ and $F_{\rm red}$ are light pressure forces acting on the atom in the field of blue- and red-detuned surface waves, respectively.

possible for a certain range of variation of the rotational quantum number: $m_{\min} \leqslant m \leqslant m_{\max}$. Outside this range, the motion is unstable.

It should be noted that the cylindrical symmetry of the optical potential is only possible for a circularly polarized field. In the case of a linearly polarized field, all three components of the electric vector are nonzero, and the optical potential does not possess cylindrical symmetry [19].

When the atom is located near the waveguide surface, the influence of van der Waals forces should also be taken into account. These forces weaken the action of the centrifugal force, which leads to a decrease in the effective potential and, as a result, the minimum of the effective potential shifts to larger values of m. Figure 4 shows the effective potentials calculated for different m, taking the van der Waals force into account [9].

3.2 Atom localization by a two-frequency light field

Figure 5 illustrates the localization geometry of an atom in a two-frequency light field [26]. The light field is formed by two light fields (both attributed to the fundamental HE_{11} mode of the nanowaveguide). One field exhibits negative frequency detuning with respect to the atomic transition frequency, while the other field has positive detuning. For the negatively detuned field, the field potential is negative, and, as a result, an atom in this potential is pulled into the strong-field region (the waveguide surface). For the positively detuned field, the potential is positive, and the atom is pulled into the weak-field region. By selecting the parameters of the light fields and nanowaveguide, we can realize the total potential having the minimum of the potential energy outside the waveguide. The atom can be localized near this minimum of the total potential.

The idea of utilizing a two-frequency light field to localize atoms was first proposed for a planar waveguide on the dielectric–vacuum boundary [28]. In this scheme, an evanescent wave with blue detuning $\delta_{\rm b} > 0$ at the interface produces a repulsive potential for an atom, while an evanescent wave with red detuning $\delta_{\rm r} < 0$ gives rise to an attraction potential. As a result, a potential well is formed between the two waves, which restricts the motion of atoms in the direction perpendicular to the interface. The red-detuned evanescent wave in a planar waveguide should have a length of penetration into the vacuum $l_{\rm r} = \alpha_{\rm r}^{-1}$ exceeding this length $l_{\rm b} = \alpha_{\rm b}^{-1}$ for the blue-detuned wave ($\alpha_{\rm r}^{-1} > \alpha_{\rm b}^{-1}$). This condition is fulfilled if the angle of incidence of the red-detuned wave only slightly exceeds the total internal reflection angle, while the angle of incidence of the blue-detuned laser wave greatly exceeds the total internal reflection angle. If this condition holds true and detunings are large, when the influence of the light pressure force can be neglected, the total potential for atoms along the z-axis perpendicular to the interface is the sum of two potentials:

$$U(\mathbf{r}) = U_{\rm gr}^{\rm b} - U_{\rm gr}^{\rm r} = \hbar\left[\frac{g_{0\rm b}^2}{\delta_{\rm b}}\exp\left(-2\alpha_{\rm b}z\right) - \frac{g_{0\rm r}^2}{|\delta_{\rm r}|}\exp\left(-2\alpha_{\rm r}z\right)\right], \tag{4}$$

where $g_{0\rm b}$ and $g_{0\rm r}$ are the interaction constants at the dielectric–vacuum boundary for blue- and red-detuned waves, respectively.

Such an atomic waveguide ensures the localization of cold atoms in a plane parallel to the dielectric–vacuum interface. When using Gaussian laser beams, this atomic waveguide can be transformed into a three-dimensional trap, because the dominating gradient force produced by the red-detuned Gaussian beam can pull atoms into the radiation trapping region.

In the case of a nanowaveguide, the question arises of whether it is possible to realize a similar situation with the minimum of the total potential near the waveguide surface. If the introduced light fields are circularly polarized (ensuring the cylindrical symmetry of the problem) and field frequencies are strongly detuned from the atomic absorption frequency, the optical potential of each of the two modes can be represented in the form

$$U_i = \frac{\hbar\Omega_i^2}{\Delta_i}, \tag{5}$$

where Ω_i is the Rabi frequency for the ith mode, and $i = 1, 2$.

For a strong enough field with a blue detuning, the total potential is repulsive near the waveguide surface and attractive at larger distances from the surface. If the characteristic time of the atomic motion greatly exceeds the beat period of two light fields, the total atomic potential is the

sum of two potentials, namely

$$U = U_1 + U_2 \approx G_2 K_0^2(q_2 r) - G_1 K_0^2(q_1 r)\,. \qquad (6)$$

The parameters of the surface potential (its depth and its minimum position) can be changed by varying laser field parameters (G_1, G_2, ω_1, ω_2) and waveguide parameters (q_1, q_2, n). The increase in G_2 and q_2, for G_1 and q_1 being fixed, leads to an increase in the depth of the potential well. Under these conditions, the bottom of the potential well is displaced to the waveguide surface.

When the radius of the fiber is small enough, the decay length of the wave is a rapidly increasing function of the wavelength of light. Therefore, by using a waveguide with a small diameter, we can attain a large ratio of q_2 to q_1 by selecting a small wavelength λ_2 and a large wavelength λ_1. Thus, by decreasing the wavelength of the blue wave or increasing the wavelength of the red wave, we can considerably increase the depth of the potential well (for appropriate laser field powers). In this case, the wavelength λ_2 should not be too small because of restrictions on the single-mode propagation of light in the waveguide. In addition, the wavelength λ_1 should not be too large, because a large wavelength leads to a large decay length $l_1 = 1/q_1$ and, therefore, to a smaller value of the potential for the same radiation power.

When an atom is located near the waveguide surface, it is also necessary to take into account the influence of van der Waals forces. Figure 6 plots the effective potentials calculated taking into account the van der Waals force. The parameters of a silica nanowaveguide are as follows: $\lambda_1 = 1.06$ μm, $\lambda_2 = 700$ nm, and the radius $a = 0.2$ μm. The blue laser power is $P_2 = 29$ mW, and the red laser powers P_1 are presented in Fig. 6. The potential minimum is located at a distance of $0.3a$.

The characteristics of light fields also affect such important parameter as the coherence time of an atom in a trap. The main factor restricting the coherence time of the atom is the spontaneous scattering of photons of localizing fields by the atom. The lifetime of the atom in a potential well of depth U_D is determined by the expression

$$\tau_{\rm trap} = \frac{U_D}{2\sum_i R_i^{\rm rec} \Gamma_i^{\rm sc}(r_{\rm m})}\,, \qquad (7)$$

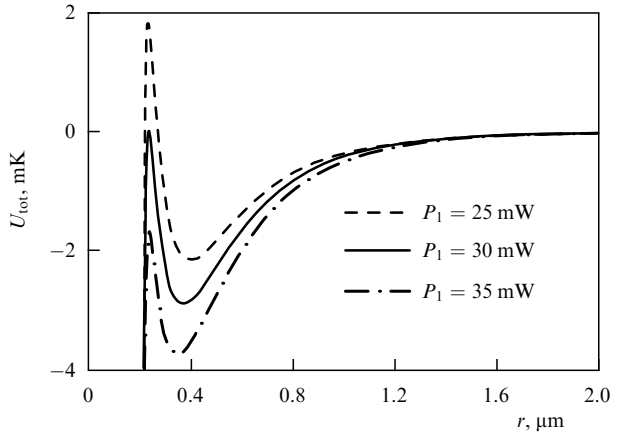

Figure 6. Optical potentials of an atom in a two-frequency light field, calculated taking into account the van der Waals force [26].

where $\Gamma_i^{\rm sc}$ is the emission rate of spontaneous photons of the light field E_i, and $r_{\rm m}$ is the distance at which the potential U_D takes the minimum value.

3.3 Experimental localization of atoms in a two-frequency light field

The localization of atoms near a nanowaveguide was first demonstrated by the A Rauschenbeutel group in a two-frequency scheme [29, 30, 46]. The optical potential (for Cs atoms) was produced by two lasers emitting at 1064 nm (pulling potential) and 780 nm (repulsive potential). The depth of the optical potential was about 100 μK. The diagnostics of atoms captured by the optical potential was made by a third laser beam resonant with the atomic transition. Figure 7a shows schematically a nanowaveguide with atoms localized around it, and Fig. 7b displays the cloud of atoms localized around the nanowaveguide. The number of localized atoms reaches about 2000, and their mean distance from the waveguide surface is about 200 nm.

The next important step in the development of techniques for controling atomic motion on the nanoscale is the experiment of the J Kimble group (California Institute of Technology) [31]. The authors of this work demonstrated the internal state-independent localization of *single* Cs atoms near a nanowaveguide surface. In the most general case, the optical potential localizing an atom has the form [32]

$$H = V_{\rm hfs} + V_{\rm EE} + V_B\,, \qquad (8)$$

where the terms $V_{\rm hfs}$, $V_{\rm EE}$, and V_B on the right-hand side depend on the hyperfine splitting, Stark interaction (light shift), and interaction with an external magnetic field, respectively. The light shift $V_{\rm EE}$ of the atomic level $|n, J\rangle$ is given by the following expression [32]

$$V_{\rm EE} = -\frac{1}{4}\left\{\alpha_{nJ}^{\rm s} - {\rm i}\alpha_{nJ}^{\rm v}\,\frac{[\mathbf{u}^*\times\mathbf{u}]\,\mathbf{J}}{2J} + \alpha_{nJ}^{\rm t}\,\frac{3\left[(\mathbf{u}^*\mathbf{J})(\mathbf{u}\,\mathbf{J}) + (\mathbf{u}\,\mathbf{J})(\mathbf{u}^*\mathbf{J})\right] - 2\mathbf{J}^2}{2J(2J-1)}\right\} E^2\,, \qquad (9)$$

where $\alpha_{nJ}^{\rm s}$, $\alpha_{nJ}^{\rm v}$, and $\alpha_{nJ}^{\rm t}$ are the scalar, vector, and tensor atomic polarizabilities, respectively, J is the total electronic angular momentum, and E is the light field amplitude. The first term on the right-hand side of formula (9) is a scalar light shift, which is the same for all Zeeman sublevels of the atom. Contributions from the vector and tensor light shifts depend on the atomic energy level, and, due to the degeneracy of

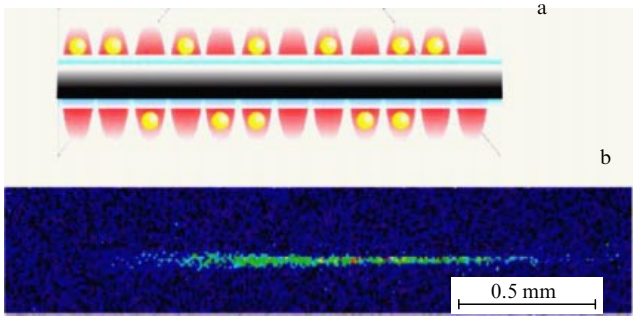

Figure 7. (a) Nanowaveguide with atoms localized around it. (b) Image of a cloud of Cs atoms localized around the nanowaveguide, obtained with a CCD camera [29].

atomic levels, the mixing of the levels is possible, resulting in the loss of atoms from the trap.

Goban et al. [31] have demonstrated in experiments the elimination of the differential scalar light shifts between the ground and excited atomic energy levels by selecting so-called magic wavelengths [33]. Magic wavelengths for Cs atoms experiencing positively and negatively detuned localizing laser fields are $\lambda_{red} = 937$ nm and $\lambda_{blue} = 686$ nm, respectively [31, 34]. In these papers, the suppression of the vector shift by a factor of 250 was also demonstrated. Atoms in such a trap experience a small perturbation at the dipole-allowed atomic transition. This allowed the observation of unbroadened resonance optical transition in localized atoms [34].

4. Atom localization by the van der Walls potential

The *optical* localization of atoms near a surface considered in Section 3 was realized at distances considerably exceeding the characteristic size of surface potentials. A similar situation also takes place in the schemes of localization of atoms in *magnetic* fields [35]. In both cases, the van der Waals interaction of atoms with the surface is either completely neglected or considered as a weak additional action on the motion of localized atoms.

The authors of Ref. [36] proposed and theoretically studied the usage of van der Waals forces in localization of neutral atoms. Because of the characteristic parameters of the potential, such a localization occurs on the nanometer spatial scale. In addition, traps based on the van der Waals potential are deeper than optical and magnetic traps. This means the presence of large energy separations between atomic levels in the trap and the possibility of realization of the single-mode regime of the atomic motion in one- and two-dimensional waveguide traps [37].

It was shown that the laser technique for manipulating atoms (cooling, localization) can be applied for the efficient loading of atoms into the surface potential. Two physical mechanisms have been proposed for this purpose. The first is based on the *photoassociation* of atoms with the surface [38], and the second on the collision energy transfer to highly excited levels (the 'energy-pooling collision' effect) [39].

The process of localization of an atom (molecule) on a surface not only is of physical interest as a whole [40] but also provides the foundation for all modern industrial micro- and nanoelectronics based on the techniques of molecular beam epitaxy or vapor-phase epitaxy [41, 42]. Therefore, the study of elementary processes of trapping particles on a surface and controling these processes are fundamentally important and have many practical applications.

The simplest surface is that of a dielectric. The proper choice of the dielectric surface allows one to exclude numerous complicating effects related to charges, currents, and chemical interactions. In addition, transparent dielectric surfaces make it possible to perform optical excitation of atoms and control them near surfaces.

An atom near the surface of a dielectric is subjected to the action of potential $V_0(z)$ formed by short-range repulsive and long-range attractive interactions:

$$V_j(z) = A_j \exp(-\alpha_j z) - \frac{C_{3j}}{z^3}. \tag{10}$$

Three interaction constants A_j, α_j, and C_{3j} depend on the dielectric material and parameters of the atom, and also on the internal state of the atom, $i = e, g$. By solving the stationary Schrödinger equation, the authors of Refs [43, 44] found the wave functions $\varphi_a(z)$ and $\varphi_b(z)$ and the energy eigenvalues E_a and E_b for the motion of the center of mass of the atom in the surface potential:

$$\left(-\frac{\hbar^2}{2m}\frac{d^2}{dz^2} + V_e(z)\right)\varphi_a(z) = E_a\varphi_a(z),$$
$$\left(-\frac{\hbar^2}{2m}\frac{d^2}{dz^2} + V_g(z)\right)\varphi_b(z) = E_b\varphi_b(z). \tag{11}$$

The energy eigenvalues E_a and E_b characterize the energy of the translatory motion of the atom in the ground and excited states. The total energies are $\hbar\omega_a = \hbar\omega_g + E_a$ and $\hbar\omega_b = \hbar\omega_e + E_b$, where $\hbar\omega_g$ and $\hbar\omega_e$ are the energies of the internal state of the atom. The states a and b for negative energies $E_a < 0$ and $E_b < 0$ are the localized states of the atom.

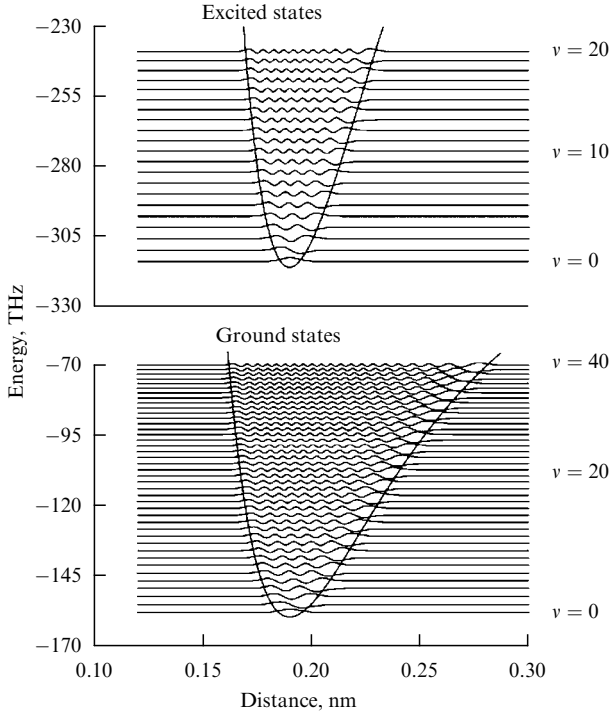

Figure 8. Energies and wave functions of the center of mass of a Cs atom moving in the surface potential [43].

Figure 8 shows the calculated energy eigenvalues and wave functions for the motion of the center of mass of the Cs atom in the surface potential [43, 44]. The maximum quantum numbers of a vibrational motion for the ground and excited states are $v_g = 311$ and $v_e = 437$, respectively. For small vibrational quantum numbers, the motion of the center of mass of the atom is strongly localized near the surface and the shift in the optical frequency of atomic absorption is considerable, reaching $\omega_0 = \omega_e - \omega_g \approx 353$ THz for Cs.

4.1 Loading of atoms into a surface potential

To trap a free atom in a potential well, a dissipative mechanism for reducing the kinetic energy of the atom is required. Thus far, two mechanisms of atom loading into a surface potential have been proposed: (i) the photoassociation of atoms [36, 38], and (ii) collision energy transfer [39].

4.1.1 Loading based on photoassociation. The photoassociation of an atom with a surface is similar to the photoassociation of two atoms. The photoassociation of atoms comprises the formation of a molecule by colliding atoms absorbing a photon during impact time. The efficient 'pairing' of atoms by light became possible only after the development of techniques for laser cooling of atoms, allowing a considerable increase in the phase density of atomic ensembles (the probability of a triple atom–atom–photon collision is proportional to the phase density of atoms $\rho\lambda_B^3$, where ρ is the density of the atoms, and λ_B is the de Broglie wavelength).

The probability of the photoassociation process can be considerably increased if one of the partners in a triple collision has a macroscopic size. Such a situation takes place in collisions of atoms with surfaces. The rate of photoassociation of an atom with a surface is many orders of magnitude higher than the corresponding rate of photoassociation of atoms (by S/λ_B^2 times, with $S/\lambda_B^2 \gg 1$, where S is the surface area irradiated by light). Nevertheless, to efficiently load atoms into a surface potential well using the photoassociation effect, ultracold atoms are required as well [36, 38].

The process of loading of an atom into the potential occurs when the free atom near a surface absorbs a laser photon and undergoes the transition to a bound state of the first excited electronic state. After absorption of the laser photon, the atom either spontaneously decays to a continuous spectrum or undergoes a transition to the ground electronic state. In the second case, the atom proves to be localized in the surface potential. By using an additional laser radiation, it is possible to realize a two-photon Raman transition resulting in the selective population of the chosen vibrational level of the ground electronic state.

The localization of atoms in the surface potential was experimentally studied utilizing a nanowaveguide [10]. The nanowaveguide was placed into a cloud of cold atoms (with the density of 0.7×10^{10} atoms per cm^3, and temperature 400 μK) confined in a magneto-optical trap (MOT). The interaction of the atoms with the nanowaveguide surface was studied by switching off the light and magnetic fields of the MOT and switching on probe laser radiation. As predicted theoretically [16] and confirmed experimentally [10, 29, 31], photons emitted by an atom can be very efficiently ($\sim 10\%$) captured by the nanowaveguide mode, which provides the detection of *single* atoms near the nanowaveguide. Therefore, the fluorescence of atoms excited by the probe laser beam could by detected by the same nanowaveguide: emitted photons were captured in the nanowaveguide and detected with a photodetector mounted at one of the waveguide ends. The fluorescent radiation signal from atoms located near the waveguide was detected as a function of the probe radiation frequency.

Figure 9a displays the possible schemes of a probe-field photon absorption by the atom: (i) absorption of the photon by the atom accompanied by the atomic transition between energy levels belonging to a continuous spectrum (in both the ground and excited electronic states); (ii) absorption of the photon accompanied by the transition between the unbound (in the ground electronic state) and bound excited electronic state of the atom, and (iii) absorption between bound states. The last case is only realized upon atom localization in the surface potential.

Figure 9b, c displays excitation spectra calculated and measured in these three cases. Calculations give evidence that the frequency-shifted broad excitation spectrum appears only when the atom *is localized* in the surface potential. Such a spectrum has been observed in experiments. The frequency shift appears due to the localization of atoms in the surface potential. The broadening is caused by the population of

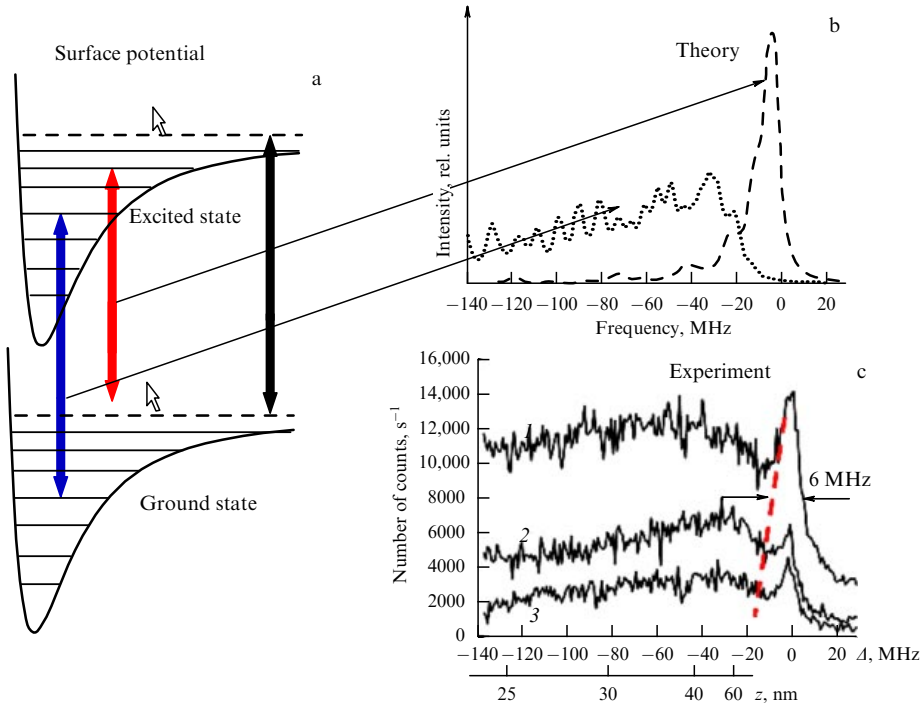

Figure 9. (Color online.) Localization of an atom in the surface potential [10]. (a) Possible optical transition diagrams between the ground and excited states of the atom: between continuous states (green arrow); between the continuous and bound states (red arrow), and between bound states (blue arrow). (b, c) Calculated and measured excitation spectra of the atom near the nanowaveguide as functions of probe radiation frequency for different probe radiation powers.

many vibrational sublevels of the potential. Thus, a comparison of absorption line profiles shows that the localization of atoms in the surface potential has been achieved in experiments.

4.1.2 Loading of atoms based on collision energy transfer. Another mechanism of loading atoms into the surface potential well is based on collision energy transfer to highly excited levels (the energy pooling collision), involving the inelastic collision of two excited atoms followed by the transition of one atom to the ground state, and the other to the excited state [39]. The atomic energy defect is compensated for by the kinetic energy of the atom. If atoms collide near the surface at a distance on the order of the potential well size and the energy defect is negative, this can lead to atomic localization in the well.

Experiment was performed with rubidium atoms [39]. Excitation of Rb atoms by a 780-nm laser leads to the population of their $5^2P_{3/2}$ levels. The 5d level is close to the $5p + 5p$ energy asymptote of the Rb_2 molecule and, consequently, it can be populated in a collision of excited atoms due to energy transfer to highly excited levels: $Rb\,(5p) + Rb\,(5p) + \Delta E \rightarrow Rb\,(5d) + Rb\,(5s)$, where $\Delta E = -93$ K is the difference between the values of the total kinetic energy before and after the collision of atoms (the energy defect). After the collision of two excited atoms, one of them undergoes the transition to the ground 5s state, and the other to the highly excited 5d state. The energy defect is compensated for due to the translational motion of atoms. Thus, the kinetic energy of two atoms after collision in this process decreases by 93 K. The process efficiency is estimated by the intensity of blue fluorescence appearing upon the transition of the rubidium atom from the 5d state to the 6p state from which the atom undergoes the transition to the ground 5s state accompanied by emitting photons at 420.2 and 421.6 nm. If two excited atoms collide near the bottom of the surface potential well, the kinetic energy loss in this collision can lead to the localization of the atom in the surface potential.

The localization of Rb atoms near the surface of an yttrium aluminum garnet (YAG) crystal was studied in paper [39]. Laser radiation was tuned close to the resonance with the $5^2S_{1/2} - 5^2P_{3/2}$ transition. The collision energy transfer (energy-pooling process) was observed by recording the blue emission of Rb atoms. The laser-induced trapping of Rb atoms was accompanied by the appearance of atoms on the crystal surface.

The localization of atoms was detected by the scattering of light on surface atoms. Figure 10 shows the process of atom loading into the surface potential depending on the surface irradiation time. The light intensity scattered by surface atoms is plotted on the ordinate, which is proportional to the number of localized atoms in the surface potential. One can see that, when laser radiation is switched off (at the moment $t = 10^4$ s), the number of atoms in the trap begins to decrease due to their thermal desorption from the surface with the characteristic time $t_d = 10^3$ s.

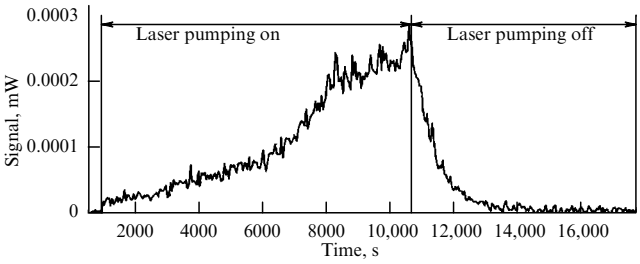

Figure 10. Loading of Rb atoms into the surface potential as a function of the laser irradiation time t [39].

5. Conclusions

Consider in conclusion a number of possible applications of the atom + nanowaveguide hybrid system. One of the most interesting applications is the use of this system for quantum information communication and processing. As shown theoretically [14, 43] and demonstrated experimentally [10, 46, 48], the spontaneous radiation of an atom (near a nanowaveguide) is efficiently coupled with the nanowaveguide mode. This, in turn, means that the nanowaveguide provides an efficient dipole–dipole interaction between two atoms at large distances (compared to the wavelength of light) [45, 47, 49]. In the case under study, the element of the quantum information network is a system of two atoms (two nodes of the quantum information network) and photons in the nanowaveguide, which provide the efficient connection between the nodes of the quantum information network.

A switch in any information device is one of the key elements. In optical waveguides, they perform switching of optical signals between different waveguides in optical communication devices. The scaling of such switches for quantum technologies means the possibility of controling optical signals (at the level of single photons) with the help of single quantum systems (atoms, molecules, quantum dots). Optical nanowaveguides and atoms near their surfaces can serve as such switches in a quantum information network.

The operation of a quantum switch was demonstrated in paper [50]. The key element in this device comprises a nanowaveguide resonator coupled with a single atom located near its surface. The nanowaveguide resonator is also coupled via a surface wave with two other nanowaveguides. Light from one nanowaveguide is delivered through the nanowaveguide resonator to another nanowaveguide. A *single atom* in this device controls the light flux between nanowaveguides, because the presence of the atom near the resonator shifts its resonance frequency, thereby changing the coupling between the nanowaveguide and resonator.

References

1. Kimble H J *Nature* **453** 1023 (2008)
2. Hammerer K, Sørensen A S, Polzik E S *Rev. Mod. Phys.* **82** 1041 (2010)
3. Miller R et al. *J. Phys. B At. Mol. Opt. Phys.* **38** S551 (2005)
4. Haroche S, Raimond J-M *Exploring the Quantum: Atoms, Cavities and Photons* (Oxford: Oxford Univ. Press, 2006)
5. Darquié B et al. *Science* **309** 454 (2005)
6. Wrigge G et al. *Nature Phys.* **4** 60 (2008)
7. Akimov A V et al. *Nature* **450** 402 (2007)
8. Tey M K et al. *Nature Phys.* **4** 924 (2008)
9. Balykin V I et al. *Phys. Rev. A* **70** 011401(R) (2004)
10. Nayak K P et al. *Opt. Express* **15** 5431 (2007)
11. Vetsch E et al. *Phys. Rev. Lett.* **104** 203603 (2010)
12. Goban A et al., arXiv:1203.5108
13. Kien F L, Dutta Gupta S, Balykin V I, Hakuta K *Phys. Rev. A* **72** 032509 (2005)
14. Kien F L, Balykin V I, Hakuta K *Phys. Rev. A* **73** 013819 (2006)
15. Liebermeister L et al. *Appl. Phys. Lett.* **104** 031101 (2014); arXiv: 1309.0421

16. Kien F L et al. *Phys. Rev. A* **72** 063815 (2005)
17. Chang D E et al. *New J. Phys.* **14** 063003 (2012)
18. Tong L et al. *Nature* **426** 816 (2003)
19. Kien F L, Liang J Q, Hakuta K, Balykin V I *Opt. Commun.* **242** 445 (2004)
20. Kien F L, Balykin V I, Hakuta K *Phys. Rev. A* **73** 053823 (2006)
21. Jackson J D *Classical Electrodynamics* 3rd ed. (New York: Wiley, 1999)
22. Padgett M, Barnett S M, Loudon R *J. Mod. Opt.* **50** 1555 (2003)
23. Allen L, Padgett M J, Babiker M *Prog. Opt.* **39** 291 (1999)
24. Allen L, Rubinsztein-Dunlop H, Ertmer W (Eds) "Special issue: Atoms and angular momentum of light" *J. Opt. B Quantum Semiclass. Opt.* **4** S1 (2002)
25. Kien F L, Balykin V I, Hakuta K *Phys. Rev. A* **74** 033412 (2006)
26. Kien F L, Balykin V I, Hakuta K *Phys. Rev. A* **70** 063403 (2004)
27. Sagué G, Baade A, Rauschenbeutel A *New J. Phys.* **10** 113008 (2008)
28. Ovchinnikov Y B, Shul'ga S V, Balykin V I *J. Phys. B At. Mol. Opt. Phys.* **24** 3173 (1991)
29. Vetsch E et al. *Phys. Rev. Lett.* **104** 203603 (2010)
30. Dawkins S T et al. *Phys. Rev. Lett.* **107** 243601 (2011)
31. Goban A et al. *Phys. Rev. Lett.* **109** 033603 (2012)
32. Kien F L, Schneeweiss P, Rauschenbeutel A *Phys. Rev. A* **88** 033840 (2013)
33. Kien F L, Balykin V I, Hakuta K *J. Phys. Soc. Jpn.* **74** 910 (2005)
34. Lacroute C et al. *New J. Phys.* **14** 023056 (2012)
35. Fortágh J, Zimmermann C *Rev. Mod. Phys.* **79** 235 (2007)
36. Lima E G et al. *Phys. Rev. A* **62** 013410 (2000)
37. Dowling J P, Gea-Banacloche J *Adv. Atom. Mol. Opt. Phys.* **37** 1 (1996)
38. Passerat de Silans T et al. *Appl. Phys. B* **82** 367 (2006)
39. Afanasiev A E, Melentiev P N, Balykin V I *JETP Lett.* **86** 172 (2007); *Pis'ma Zh. Eksp. Teor. Fiz.* **86** 198 (2007)
40. Zhang Z, Lagally M G *Science* **276** 377 (1997)
41. Capasso F (Ed.) "Special issue: Nanoscale and ultrafast devices" *Phys. Today* **43** (2) (1990)
42. Aseev A L *Ross. Nanotekhnol.* **1** (1–2) 97 (2006)
43. Kien F L, Hakuta K *Phys. Rev. A* **75** 013423 (2007)
44. Kien F L, Dutta Gupta S, Hakuta K *Phys. Rev. A* **75** 062904 (2007)
45. Nayak K et al., in *Quantum Electronics and Laser Science Conf., Long Beach, Calif., USA, May 21, 2006. Technical Digest*, paper QThC3
46. Junge C et al. *Phys. Rev. Lett.* **110** 213604 (2013)
47. Chang D E et al. *New J. Phys.* **14** 063003 (2012)
48. Chang D E, Cirac J I, Kimble H J *Phys. Rev. Lett.* **110** 113606 (2013)
49. Kien F L et al. *Phys. Rev. A* **72** 063815 (2005)
50. O'Shea D et al. *Phys. Rev. Lett.* **111** 193601 (2013)

PACS numbers: **87.64.–t**, 87.85.Qr, 87.85.Rs
DOI: 10.3367/UFNe.0184.201406i.0665

Structural nucleic acid nanotechnology: liquid-crystalline approach

Yu M Yevdokimov, O N Kompanets

1. Introduction

Bionanotechnology constitutes a branch of nanotechnology aimed at the creation of spatial nanoconstructions (nano-objects) possessing dimensional properties and made up of the molecules of biological origin as 'building blocks' [1]. Despite the diversity of biological molecules, real practical results have been obtained so far only in one direction of bionanotechnology, namely, in *nucleic acid nanotechnology*. The last technology is aimed at building the spatial objects (nanostructures and nanoconstructions) with controllable properties, which are made of nucleic acid (NA) molecules or their complexes. This area of bionanotechnology is also called *structural nucleic acid nanotechnology* [2].

In this paper, we consider the basic principles of the liquid-crystalline approach to creating spatial nanoobjects based on double-stranded DNA (deoxyribonucleic acid) molecules with different properties. The physical chemistry of polymers, including nucleic acids and their complexes, shows that a few scenarios of creating such nanoobjects are possible, taking into account the concept of the ordering of neighboring double-stranded NA molecules in particles of liquid-crystalline dispersions.[1]

2. 'Liquid' particles in liquid-crystalline dispersions based on double-stranded DNA molecules

It is known that the phase exclusion of rigid, linear, double-stranded NA molecules [3] with a molecular mass smaller than 1×10^6 Da from the aqueous salt solutions of some polymers, for example, poly(ethyleneglycol) (PEG), is accompanied by the formation of NA dispersions. The phase exclusion efficiency depends on a number of factors indicated in Fig. 1. Two factors, the molecular mass and solubility of double-stranded DNA molecules, are especially important. The higher the molecular mass of DNA, the lower the compatibility of this molecule with the PEG solution, and the higher the phase exclusion efficiency. The lower the solubility of DNA molecules, the higher their immiscibility with a PEG solution and the higher the phase exclusion efficiency [3].

Theoretical estimates based on the application of various methods (sedimentation analysis, scattering of UV radiation, dynamic light scattering, etc.) have shown that for double-stranded DNA molecules with the molecular mass $(0.6-0.8) \times 10^6$ Da, the mean diameter of dispersion particles is close to 500 nm. The molecular mass of one dispersion particle reaches $\sim 10^{10}$ Da, i.e., a particle contains approximately 10^4 DNA molecules [3].

Dispersion particles have several characteristic features. First, a polymer is not contained in dispersion particles. Second, neighboring DNA molecules are separated by a distance of 2.5–5.0 nm, i.e., particles have properties typical for crystals; in addition, neighboring DNA molecules are mobile, i.e., particles possess the property inherent in fluid. These facts allow one to describe such particles using the terms *liquid-crystalline dispersions* (LCDs) or even a DNA *liquid particle*. Third, the interaction between neighboring

Yu M Yevdokimov Engelgardt Institute of Molecular Biology, Moscow, Russian Federation
E-mail: yevdokim@eimb.ru
O N Kompanets Institute of Spectroscopy, RAS, Troitsk, Moscow, Russian Federation
E-mail: onkomp@isan.troitsk.ru

Uspekhi Fizicheskikh Nauk **184** (6) 665–672 (2014)
DOI: 10.3367/UFNr.0184.201406i.0665
Translated by M Sapozhnikov; edited by A Radzig

[1] Disperse systems comprise microheterogeneous systems with a strongly developed interface between phases, consisting of two or more phases, at least one of them (the disperse phase) being distributed in the surrounding continuous disperse medium — gas, liquid, or solid — in the form of small particles (crystal particles, drops, bubbles). Instead of the term 'disperse phase', simply the word 'dispersion' is often used. Also, expressions 'polymer dispersions' or 'liquid-crystalline dispersions' are commonly used in chemistry.